Clays and Clay Minerals, Vol. 58, No. 1, 62–71, 2010.

STACKING DISORDER IN A SEDIMENTARY KAOLINITE

TOSHIHIRO KOGURE[1,*], JESSICA ELZEA-KOGEL[2], CLIFF T. JOHNSTON[3], AND DAVID L. BISH[4]

[1] Department of Earth and Planetary Science, Graduate School of Science, The University of Tokyo, 7-3-1 Hongo, Bunkyo-ku, Tokyo, 113-0033, Japan
[2] IMERYS, Sandersville, GA 31082, USA
[3] Crop, Soil and Environmental Sciences, Purdue University, 915 W. State Street, West Lafayette, IN 47907-2054, USA
[4] Department of Geological Sciences, Indiana University, Bloomington, IN 47405, USA

Abstract—Although structural disorder in kaolinite has been investigated extensively, it is still not understood properly. To investigate the problem, a kaolinite specimen of sedimentary origin from Capim, Brazil, was examined, mainly by transmission electron microscopy (TEM). Selected-area electron diffraction (SAED) along the X_i ([100], [110], and [1$\bar{1}$0]) directions shows various features, from completely discrete patterns to heavily streaked ones along the $\boldsymbol{c}^*$ direction, suggesting that the degree of stacking disorder is variable among individual grains. High-resolution TEM images indicate that stacking faults are mainly caused by disorder of alternating $\boldsymbol{t}_1$ (~$-\boldsymbol{a}/3$) and $\boldsymbol{t}_2$ ($-\boldsymbol{a}/3 + \boldsymbol{b}/3$) layer displacements. Furthermore, stacking faults have been observed (1) as isolated stacking faults (*e.g.* insertion of an isolated $\boldsymbol{t}_2$ 'fault' in an ordered sequence with $\boldsymbol{t}_1$ layer displacement) and (2) as interstratification of two kinds of multilayer blocks having regular $\boldsymbol{t}_1$ and $\boldsymbol{t}_2$ layer displacements. A mixture of grains with various degrees and modes of disorder with alternating $\boldsymbol{t}_1$ and $\boldsymbol{t}_2$ layer displacements may explain the experimental profile of the 02, 11 X-ray diffraction band.

Faults related to displacement of the octahedral vacancy and/or to layer rotation were also observed in HRTEM images. The SAED patterns along the Y_i ([010], [310], and [3$\bar{1}$0]) directions occasionally have extra spots and/or streaks, suggesting the presence of stacking sequences with (±60º, 180º) mutual layer rotation and/or with (0, $\pm\boldsymbol{b}/3$) layer displacements. The local dickite or nacrite-like fragments formed by these faults are in qualitative agreement with recent low-temperature FTIR results from this sample, where distinct ν(OH) absorption bands reflect multiple interlayer O–H···O environments that are possibly ascribed to dickite and nacrite.

Key Words—FTIR, HRTEM, Kaolinite, SAED, Stacking Fault.

INTRODUCTION

Structural defects in kaolinite, $Al_2Si_2O_5(OH)_4$, have been investigated intensively because of the geologic and industrial importance of the mineral. In particular, the nature and degree of stacking disorder in kaolinite have been of sustained interest during the past half century. A number of quantitative models have been proposed to describe stacking disorder in kaolinite (*e.g.* Brindley and Robinson, 1946; Murray, 1954; Plançon and Tchoubar, 1977; Giese, 1988; Bookin *et al*., 1989; Zvyagin and Drits, 1996; Plançon, 2001; Reynolds and Bish, 2002) including $\pm\boldsymbol{b}/3$ random layer displacement (Brindley and Robinson; 1946), ±120º mutual layer rotation (Murray, 1954), and displacement of octahedral vacancy sites in the dioctahedral sheet (Plançon and Tchoubar, 1977). Because kaolinite occurs as fine particles, powder X-ray diffraction (XRD) is the most convenient and useful technique for its crystallographic characterization. Stacking disorder in kaolinite degrades the observed XRD patterns in predictable ways depending on the degree and nature of the disorder. The accuracy of these models has been assessed by evaluating how well the simulated XRD patterns reproduce experimental ones. Bookin *et al.* (1989) considered layer distortions in the kaolinite layer and discussed the possibility of the occurrence of these stacking disorder models. They also found that the kaolinite layer contains a pseudo-mirror plane passing through the octahedral vacancy site and proposed a stacking disorder model with two alternating layer displacements, $\boldsymbol{t}_1$ (~$-\boldsymbol{a}/3$) and $\boldsymbol{t}_2$ ($-\boldsymbol{a}/3 + \boldsymbol{b}/3$) that are related to each other by this pseudo-mirror plane. Zvyagin and Drits (1992) deduced possible variants of stacking faults in kaolinite based on the structural features of kaolin-group minerals, following the discussion in Bookin *et al.* (1989). Plançon *et al.* (1989) reported that XRD patterns of many kaolinite specimens were reproduced by a model in which alternating $\boldsymbol{t}_1$ and $\boldsymbol{t}_2$ layer displacements induce the main stacking disorder/fault and insertion of the layer with the octahedral vacancy at the *C* site (*C* layer) as the minor fault. Plançon *et al.* (1988, 1989) suggested that two assemblages of kaolinite particles differing from each other by their degree of structural disorder are necessary to reproduce inter-peak intensities in the 02, 11 band in the XRD patterns from a number of kaolinite specimens with Hinckley index (Hinckley, 1963) > 0.4.

* E-mail address of corresponding author:
kogure@eps.s.u-tokyo.ac.jp
DOI: 10.1346/CCMN.2010.0580106

https://doi.org/10.1346/CCMN.2010.0580106 Published online by Cambridge University Press

Kogure and Inoue (2005a) succeeded in determining the stacking-fault structures directly from HRTEM images of a kaolinite specimen of diagenetic origin, overcoming the difficulty in recording HRTEM images due to rapid radiation damage. They reported that most faults observed in this kaolinite specimen were caused by alternating $\boldsymbol{t}_1$ and $\boldsymbol{t}_2$ layer displacements, in accordance with the suggestion by Bookin *et al*. (1989) and Plançon *et al.* (1989). Kogure and Inoue (2005b) examined the stacking disorder in a dickite-dominant specimen of hydrothermal origin using HRTEM, in which they found the coexistence of the two types of defects, disorder of the layer displacements and octahedral vacancy sites. They also found several long-period polytypes of kaolin-group minerals, indicating that the crystals were formed by spiral growth.

Johnston *et al*. (2008) examined various kaolinite specimens using low-temperature FTIR spectroscopy at 15 K and reported that spectra from several specimens showed absorption bands that can be assigned to dickite and nacrite, in addition to those of kaolinite. Of particular interest was a sedimentary kaolinite from Brazil which originates from weathering near the surface and has not experienced high-temperature conditions. This sample also showed the spectral features ascribed to dickite- and nacrite-like stacking sequences that are considered as high-temperature polytypes (*e.g*. Ehrenberg *et al*., 1993). However, the FTIR data were unclear as to whether these sequences exist as separate phases or as stacking disorder.

In the present study, a kaolinite specimen investigated by Johnston *et al*. (2008) was reexamined, mainly using HRTEM, to elucidate the nature of stacking disorder and its relationship with the genesis of this mineral, as well as the correspondence with the XRD pattern and FTIR spectrum.

SAMPLE AND METHODS

The specimen investigated was a 'soft kaolin' from the Amazon basin of northern Brazil, referred to as Capim kaolin (Sousa *et al*., 2007). After gentle grinding, the sample was dispersed with sodium hexametaphosphate and centrifuged to isolate the 2−5 μm fraction (Johnston *et al*., 2008). A powder XRD pattern was collected using a Rigaku RINT-Ultima$^+$ diffractometer with CuKα radiation, graphite monochromator, 0.3 mm receiving slit, and 1.0º divergence and anti-scatter slits. A continuous scan rate of 0.1º2θ min^{-1} and sampling interval of 0.02º were adopted

Cross-sectional specimens for TEM experiments with the electron beam parallel to [*hk*0] directions were prepared as follows. Kaolinite particles dispersed in water by ultrasonication were deposited by sedimentation onto a glass substrate to align the kaolinite plates in parallel. After drying, platy aggregates of the particles were collected and embedded between two glass slides with epoxy resin. The glass slides were then cut perpendicular to their surfaces, using a diamond wheel, to laths of ~1 mm thick. After mechanical thinning down to ~70 μm, the specimen was finally thinned by conventional argon ion milling.

Examination by HRTEM was performed at 200 kV using a JEOL JEM-2010 microscope with a UHR pole piece (C_s = 0.5 mm). After setting the crystal orientation using SAED, focus was adjusted with minimum illumination using an LH72LL-TEM TV-rate CCD camera (LHESA Electronique, Cergy, Pontoise, France). Immediately after focusing, the illumination was intensified for exposure on film. The exposure time was ~0.5−1.0 s and the direct magnification on the films was 400,000× or 500,000×. Generally, only one exposure could be obtained before the crystal deteriorated due to the radiation damage (Kogure and Inoue, 2005a). Successful images recorded on the films were digitized using a CCD camera. Noisy contrast from amorphous materials in the images was removed using a Wiener filter (Marks, 1996; Kilaas, 1998) developed by K. Ishizuka (HREM Research Inc., Saitama, Japan) and implemented in Gatan *DigitalMicrograph* version 3.1 0.0 (Kogure *et al*., 2008).

The recording of kaolinite crystals in the present specimen by HRTEM was more difficult than in previous studies (Kogure and Inoue, 2005a, 2005b) because of the smaller grain size (~2 μm in the present specimen compared to ~10 μm in the prior studies). Because the nature of the sample only permitted a limited amount of time for focusing, whether the contrast of the recorded image was reversed against the electrostatic potential in the crystal is uncertain. The results described in the following section are not affected by this ambiguity, however. See Kogure and Inoue (2005b) for an interpretation of the HRTEM contrast of dioctahedral 1:1 layers and for additional detail of how to analyze the stacking sequences.

RESULTS

Most peaks in the XRD pattern (Figure 1) can be assigned to kaolinite except for two weak peaks, indicated with arrows, which may be assigned to dickite (see the next section). The Hinckley index calculated from the 02, 11 band was 1.12. The peak positions for 021, 0$\bar{2}$1, 111, *etc*. were coincident with the calculated values with deviations <0.02º, using the refinement-based cell parameters of kaolinite (*e.g*. Bish and Von Dreele, 1989) (Figure 1b).

Plan-view and cross-sectional TEM images of the specimen (Figure 2) indicated that most grains show a euhedral, hexagonal shape in the plan-view image (Sousa *et al*., 2007). Platy grains were generally aligned in the cross-sectional specimen (Figure 2b) resulting from the sample preparation using sedimentation as described above, which is suitable for observations

https://doi.org/10.1346/CCMN.2010.0580106 Published online by Cambridge University Press

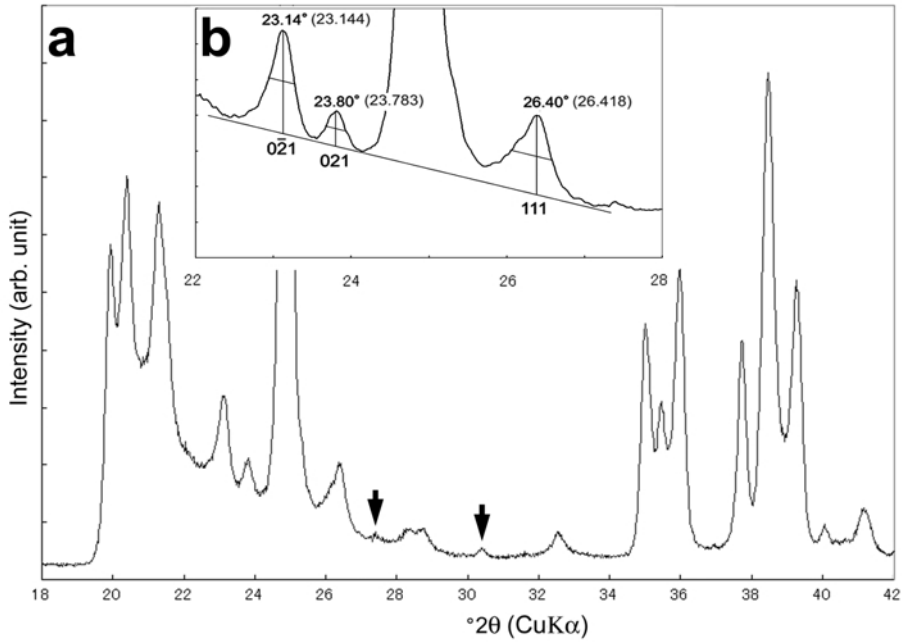


Figure 1. Powder XRD pattern of Capim kaolinite. The two peaks indicated by the arrows in (a) are unidentified. (b) Magnified pattern showing the peak profiles for the 021, 021, and 111 reflections. The figures on the peaks are the measured summit 2θ positions of the peaks whereas those in the parentheses are calculated positions using the cell constants reported by Bish and Von Dreele (1989).

along the [*hk*0] directions. The thickness of the grains was rather uniform, from 50 to 100 nm. The SAED patterns along the X_i directions (Bailey, 1963), which corresponded to the [100], [110], and [1$\bar{1}$0] directions for kaolinite, were taken from many grains using an aperture of ~100 nm diameter (Figure 3). The diffraction patterns were varied (Figure 3a–d), from almost discrete spots (Figure 3a) to continuous streaks (Figure 3d) on the first and second diffraction rows beside the 00*l*, suggesting that the degree of stacking disorder was diverse among individual grains. The pattern in Figure 3b had extra spots with streaks, implying that the selected area contained interstratification of two types of domains. On the other hand, the pattern in Figure 3c had asymmetric streaking on the two sides of the diffraction spots on 11*l* or 1$\bar{1}$*l* diffraction rows. The source of these diffraction features is discussed below.

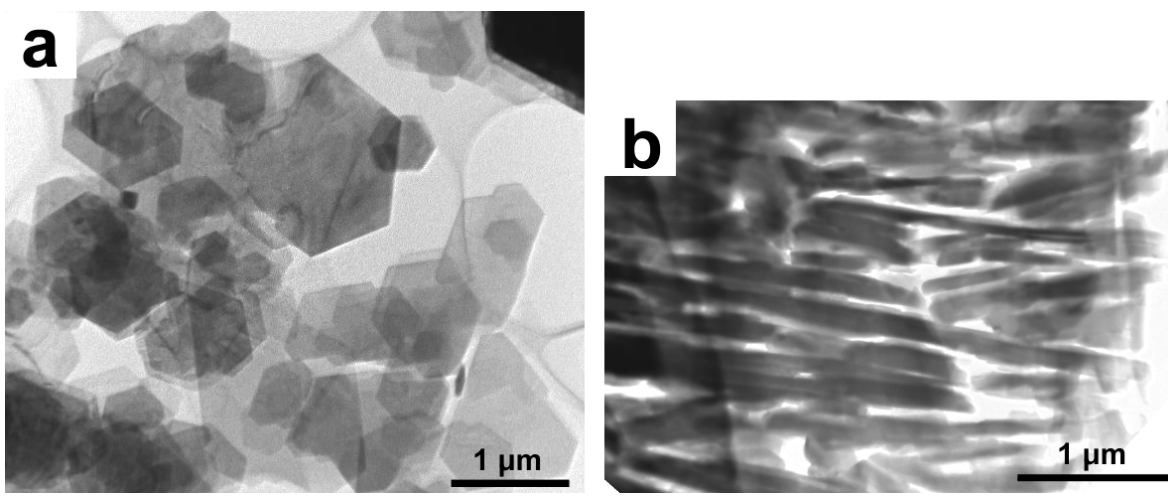


Figure 2. (a) Plan-view TEM image of Capim kaolinite dispersed on a holey carbon film. (b) Cross-sectional TEM image of the specimen. The platy crystals of kaolinite were aligned by sedimentation during sample preparation.

https://doi.org/10.1346/CCMN.2010.0580106 Published online by Cambridge University Press

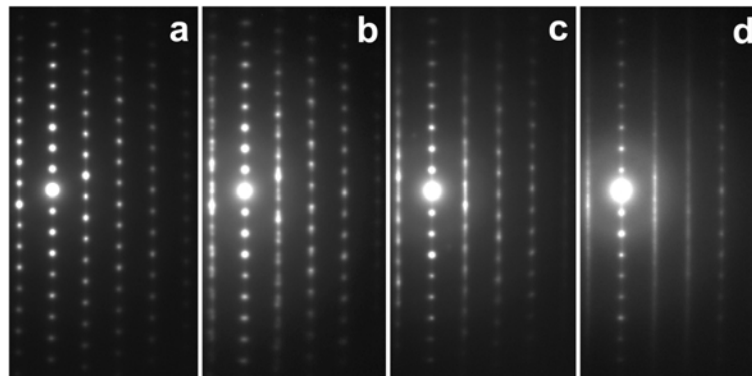


Figure 3. SAED patterns from several kaolinite crystals along the x_i directions, using an aperture of ~100 nm diameter.

A HRTEM image of a kaolinite crystal along the [110] (or [$\bar{1}$10]) direction (Figure 4a) contains several irregular contrasts parallel to the (001) plane, which corresponded to stacking faults. A more magnified image at the edge of the crystal (Figure 4b) indicated that the contrast of each kaolinite layer was identical (indicated with a triangle, see Kogure and Inoue, 2005b) but the relative position between adjacent layers was changed locally as indicated by the arrows. The stacking faults were a result of disorder of alternating $\boldsymbol{t}_1$ and $\boldsymbol{t}_2$ layer displacements, as described by Kogure and Inoue (2005a, 2005b). All faults recorded in Figure 4a were of this type. A noticeable feature is that most of these faults resulted from the isolated insertion of different layer displacement in an ordered matrix. Figure 5 shows similar features, although the density of faults is greater than in Figure 4.

In Figure 6, the stacking disorder appears different although it was also caused by alternating $\boldsymbol{t}_1$ and $\boldsymbol{t}_2$ layer displacements. The stacking may be described as a mixture of two types of multilayer blocks with regular $\boldsymbol{t}_1$ and $\boldsymbol{t}_2$ layer displacements. Such a fault structure is expected to generate an SAED pattern in which extra spots appear by the overlap of two reciprocal lattices from the different blocks. The SAED pattern in Figure 3b presumably corresponds to such a structure (recording both the HRTEM image and SAED pattern from the same area was impossible due to rapid radiation damage). On the other hand, the SAED pattern shown in Figure 3c (asymmetric streak) probably corresponds to the defect structures shown in Figures 4 and 5. Among the SAED patterns recorded, patterns such as those shown in Figure 3b,c were commonly observed, suggesting that both modes of the defect structures are common in the specimen.

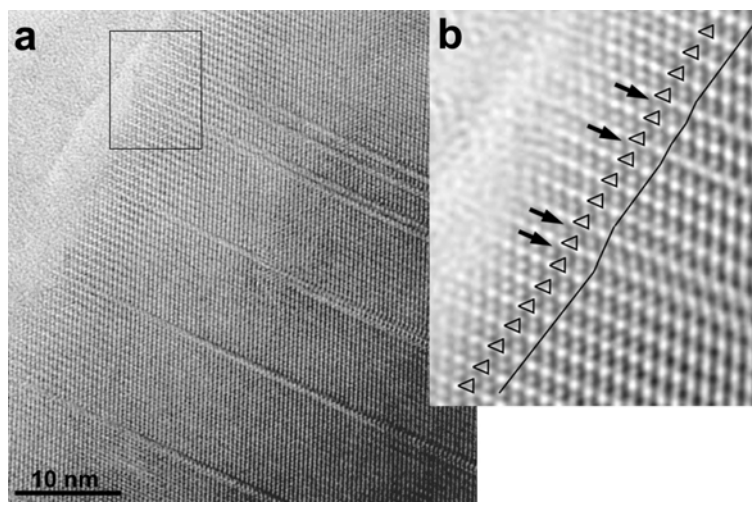


Figure 4. (a) Filtered HRTEM image of a kaolinite crystal along the [110] direction. Several stacking faults are observed as a distinct contrast parallel to the (001) plane. (b) Magnified image of the rectangle area in (a). The triangle for each layer represents the characteristics of the contrast for the kaolinite layer (Kogure and Inoue, 2005b). The solid line connects the equivalent point in each layer. The arrows indicate the stacking faults with the different layer displacement ($\boldsymbol{t}_2$ instead of $\boldsymbol{t}_1$ or *vice versa*).

https://doi.org/10.1346/CCMN.2010.0580106 Published online by Cambridge University Press

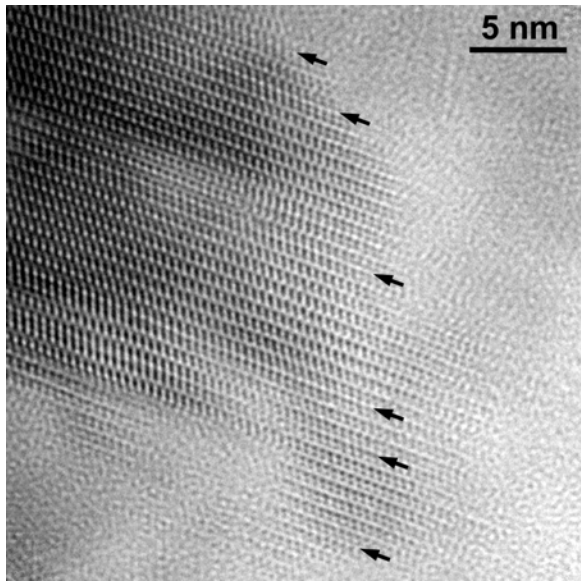


Figure 5. Filtered HRTEM image of a kaolinite crystal along the [100] direction. Stacking faults with the different layer displacement are indicated by the arrows.

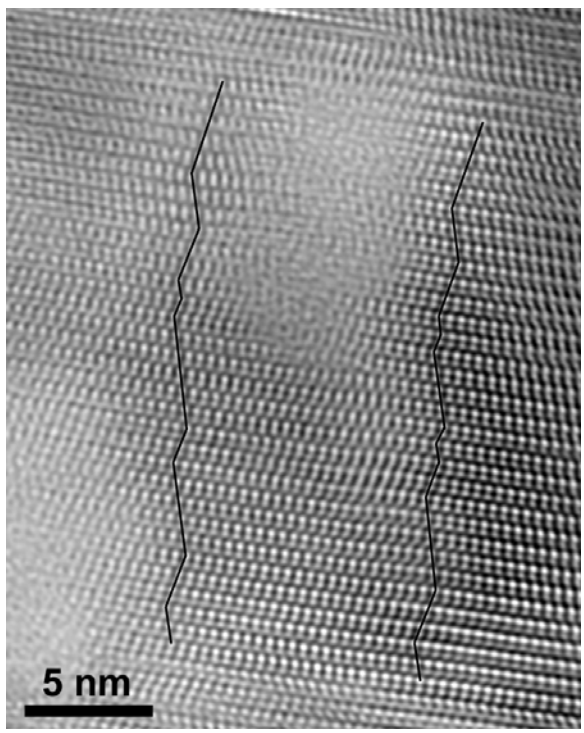


Figure 6. Filtered HRTEM image of a kaolinite crystal along one of the x_i directions. The two solid lines connect the equivalent point in each layer along the stacking. Note that the stacking structure consists almost entirely of the two kinds of multi-layer blocks with different layer displacements.

Although less common than the disorder by alternating $\boldsymbol{t}_1$ and $\boldsymbol{t}_2$ layer displacements, another type of stacking fault, where the contrast of each layer was not uniform for all kaolinite layers, was also found (Figures 7 and 8). The kaolinite layers indicated by the square brackets or arrows in Figure 7 have a contrast with white bars perpendicular to the layers in the thinnest region of the crystal, whereas the other layers have a contrast with staggered white dots, as indicated by the triangles in Figure 4b. This is due either to the displacement of the octahedral vacancy or to the rotation of adjacent layers by $n60$, $n = 1-5$. The blocks indicated by the square brackets have different directions of layer displacement as well as different contrast of the layers from those in the rest area. Hence, they are considered as

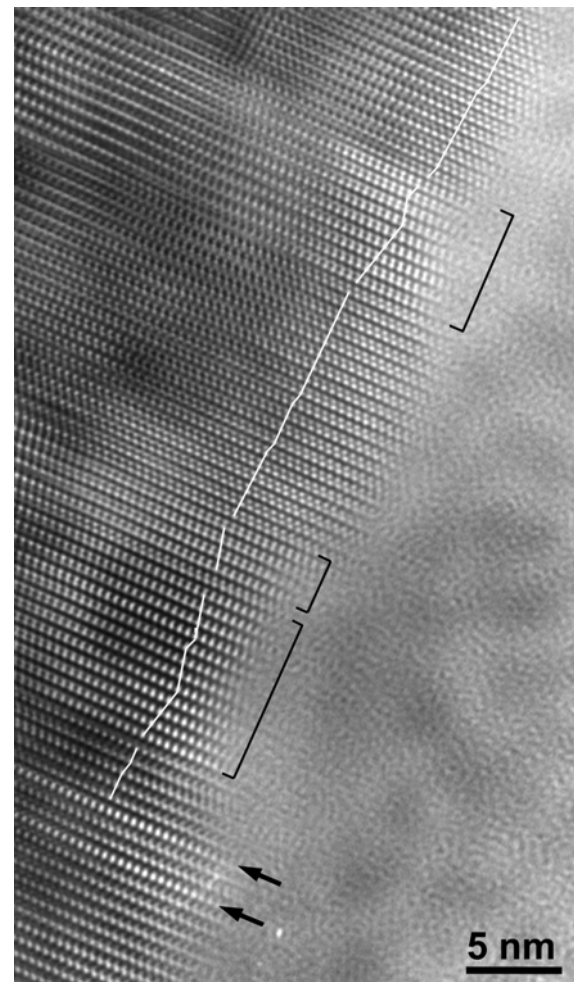


Figure 7. Filtered HRTEM image of a kaolinite crystal along one of the x_i directions. The layers indicated with the square brackets and arrows have a different contrast from the others, suggesting displacement of the octahedral vacancy site or $n60^\circ$ layer rotation. The white lines connect the equivalent point in each layer along stacking, within multi-layer blocks with the same layer contrast.

https://doi.org/10.1346/CCMN.2010.0580106 Published online by Cambridge University Press

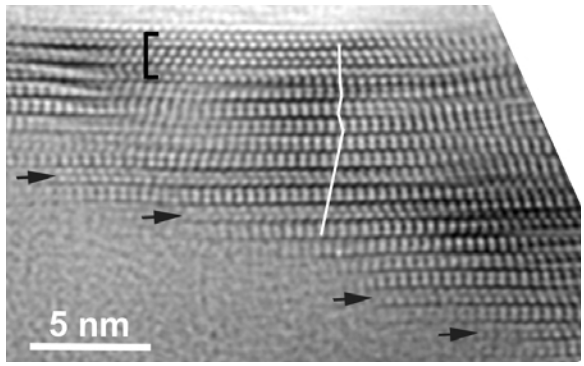


Figure 8. Filtered HRTEM image of a kaolinite crystal along one of the x_i directions. The arrows and bracket indicate layers with a different contrast from others. Note that two-layer periodicity is observed locally, implying the formation of dickite- or nacrite-like stacking. The disturbed contrast at the top right of the image is probably due to misalignment of the crystal orientation by local crystal bending.

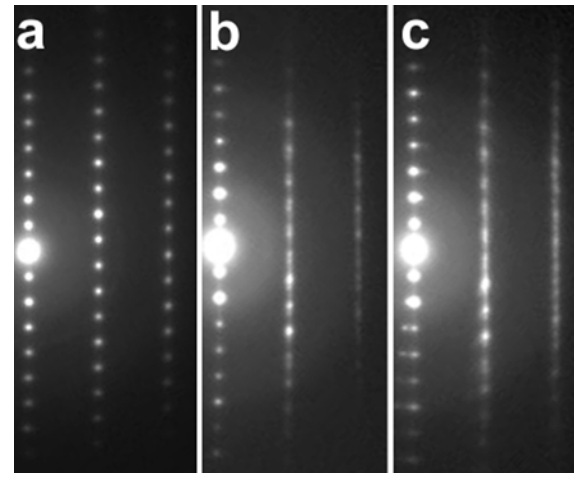


Figure 9. SAED patterns along the y_i directions of kaolinite. The pattern in (a) is common and the normal one with a regular reciprocal lattice, whereas those in (b) and (c) contain extra spots and streaks, suggesting stacking disorder with (0 or $\pm\boldsymbol{b}/3$) layer displacement and/or $(2n+1)60^\circ$ layer rotation.

rotational twins. Stacking containing a 'local' two-layer periodicity with the different layer contrasts was also observed (Figure 8). This contrast is similar to dickite or nacrite structures.

As reported by Johnston *et al*. (2008), electron diffraction patterns of the specimen recorded along the Y_i directions, or [010], [310], and [3$\bar{1}$0] of kaolinite, also indicated stacking disorder (Figure 9). As shown by Kogure and Inoue (2005b), alternation of $\boldsymbol{t}_1$ and $\boldsymbol{t}_2$ layer displacements, displacement of the octahedral vacancy among the *A*, *B*, and *C* sites (Bailey, 1963), and/or the occurrence of $2n60^\circ$ layer rotation have almost no influence on the diffraction pattern along the Y_i directions (Figure 9a). The patterns showed extra spots and/or streaks on the second and third diffraction rows (Figures 9b and 9c), indicating that the stacking sequences contained faults corresponding to (0 or $\pm\boldsymbol{b}/3$) layer displacement, and/or $(2n+1)60^\circ$ layer rotation.

To determine the actual defect types occurring in the specimen, HRTEM images along Y_i directions were necessary, as reported by Kogure *et al*. (2001) for cronstedtite. HRTEM images of kaolin-group minerals were more difficult to obtain along the Y_i direction than along the X_i direction, because the resolution required to analyze the stacking sequences was greater (<2.6 Å). Virtually all attempts failed with the exception of one imperfect image (Figure 10). Although the crystal structure almost disappeared, the two-dimensional lattice image and its Fourier transform (inset on Figure 10) prove unambiguously the existence of stacking disorder in the crystal.

DISCUSSION

The TEM experiments have revealed that the stacking disorder in the present specimen is diverse. The degree of stacking disorder is very variable among individual grains (Figure 3). Sousa *et al.* (2007) suggested that Capim kaolinite was formed by intense lateritization of sandy-clay sediments. The diversity of stacking disorder among individual grains implied that local environments to precipitate kaolinite were inhomogeneous or that it formed in a non-equilibrium manner. As mentioned above, Plançon *et al.* (1988) proposed a model with a mixture of two types of crystallites (or coherent scattering domains) having different degrees of stacking disorder to explain the inter-peak intensity in the 02, 11 band. However, the degrees of stacking disorder appear to be much more variable among the crystallites, although the limited number of grains examined by SAED precludes a quantitative comparison with XRD data.

Among the different types of faults, that corresponding to alternating $\boldsymbol{t}_1$ and $\boldsymbol{t}_2$ layer displacements was most abundant. The two layer displacements are related to each other by the pseudo-mirror plane in the kaolinite layer, and the structures with $\boldsymbol{t}_1$ and $\boldsymbol{t}_2$ layer displacements are thus enantiomers (Bookin *et al*., 1989). Two extreme modes of occurrence of this type of defect have been observed (Figures 4–6). In the paper by Kogure and Inoue (2005a), all HRTEM images from a diagenetic kaolinite specimen showed stacking disorder similar to that in Figure 6, an interstratification of two kinds of multilayer blocks having regular $\boldsymbol{t}_1$ and $\boldsymbol{t}_2$ layer displacements. Bookin *et al.* (1989) described the stacking disorder illustrated in Figures 4 and 5 as 'mechanical displacement' and that in Figure 6 as 'growth faults.' However, whether the stacking disorder shown in Figures 4 and 5 were actually formed 'mechanically' by an external force after crystallization

https://doi.org/10.1346/CCMN.2010.0580106 Published online by Cambridge University Press

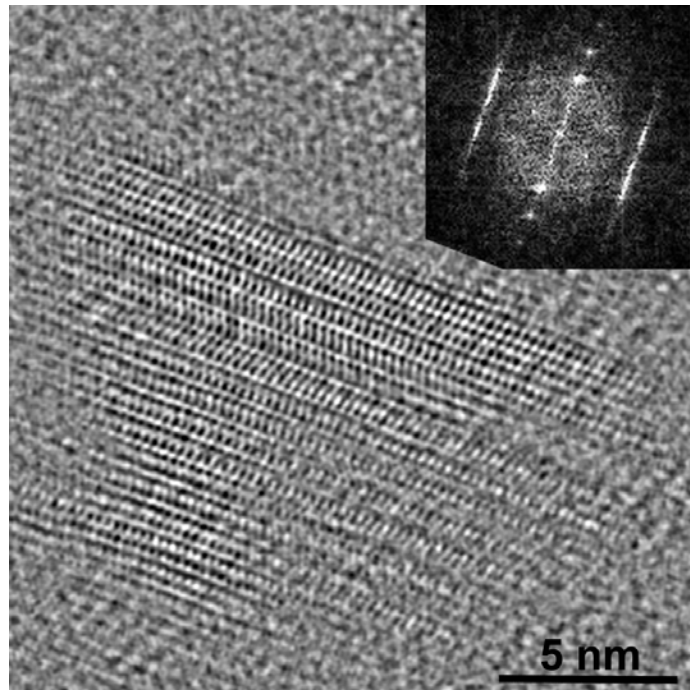


Figure 10. Filtered HRTEM image of a kaolinite crystal along one of the y_i directions. The crystal was damaged by electron radiation (making it amorphous) except for the central region. The inset is the Fourier transform of the image, showing stacking disorder in the image.

is unclear. The two types of stacking disorder are thus referred to hereafter as 'isolated faults' (IF) and 'enantiomeric twins' (ET).

Bookin *et al.* (1989) simulated XRD patterns to estimate how IF and ET defects affect the XRD profiles. Unfortunately, their results are confusing, having been published with editorial errors. In addition, the parameters used for their calculations are not adequate for comparison with the present data. Hence, XRD patterns for IF and ET defects, according to the description by Bookin *et al*. (1989), were also calculated here by simulation using the *DIFFaX* program (Treacy *et al*., 1991). In the simulation, a layer with $\boldsymbol{t}_1$ displacement was named layer 1 and the equivalent layer, but with layer displacement of $\boldsymbol{t}_2$, as layer 2. The ratio of the number of each layer in the stacking sequence was expressed as W_1:W_2, and the junction probabilities were expressed as P_{ij} (i,j = 1, 2) *i.e*. a 2×2 matrix (Reichweite = 1). Among these six parameters, two were independent as $W_1 + W_2 = 1$, $P_{11} + P_{12} = 1$, $P_{21} + P_{22} = 1$, and $W_1 \times P_{12} = W_2 \times P_{21}$.

P_{ij} in IF mode were expressed as

$$\begin{pmatrix} P_{11} & P_{12} \\ P_{21} & P_{22} \end{pmatrix} = \begin{pmatrix} 1-p & p \\ 1 & 0 \end{pmatrix}$$

with p (= P_{12}) $\leqslant$ 0.5. The p is the junction probability from layer 1 to layer 2 and equivalent to the ratio of layers 1 and 2 ($p = W_2/W_1$) in this case. On the other hand, assuming $W_1 = W_2$ in ET mode, values for P_{ij} could be expressed as

$$\begin{pmatrix} P_{11} & P_{12} \\ P_{21} & P_{22} \end{pmatrix} = \begin{pmatrix} 1-p & p \\ p & 1-p \end{pmatrix}$$

where p ($= P_{12} \leqslant 0.5$) is equivalent to the inverse of the average number of layers in a block. The influence of p, which expresses the degree of stacking disorder in each mode upon several reflections of the 02, 11 band in the XRD patterns, is shown in Figure 11. The peak position and width of other reflections in the band were also affected by the disorder but the degree of their peak shift and broadening was less than those of the reflections shown in Figure 11 (Plançon and Zacharie, 1990). Disorder in ET mode broadens the 021, $0\bar{2}1$, and 111 peaks but does not change their peak positions unless p becomes larger (0.3). On the contrary, disorder in IF mode shifts the peak positions to a larger (021 and 111) or smaller ($0\bar{2}1$) angle, and broadens the peaks. These peak shifts were expected quantitatively because insertion of the layers with $\boldsymbol{t}_2$ layer displacement in the ordered stack of layers with $\boldsymbol{t}_1$ displacement alters the 'average' α and β angles of the crystal (see the schematic figure in the right of Figure 11b).

As mentioned, the positions of experimental 021, $0\bar{2}1$, and 111 peaks in the XRD pattern were not shifted within precision (Figure 1b), suggesting the prevalence of highly ordered grains or the presence of

https://doi.org/10.1346/CCMN.2010.0580106 Published online by Cambridge University Press

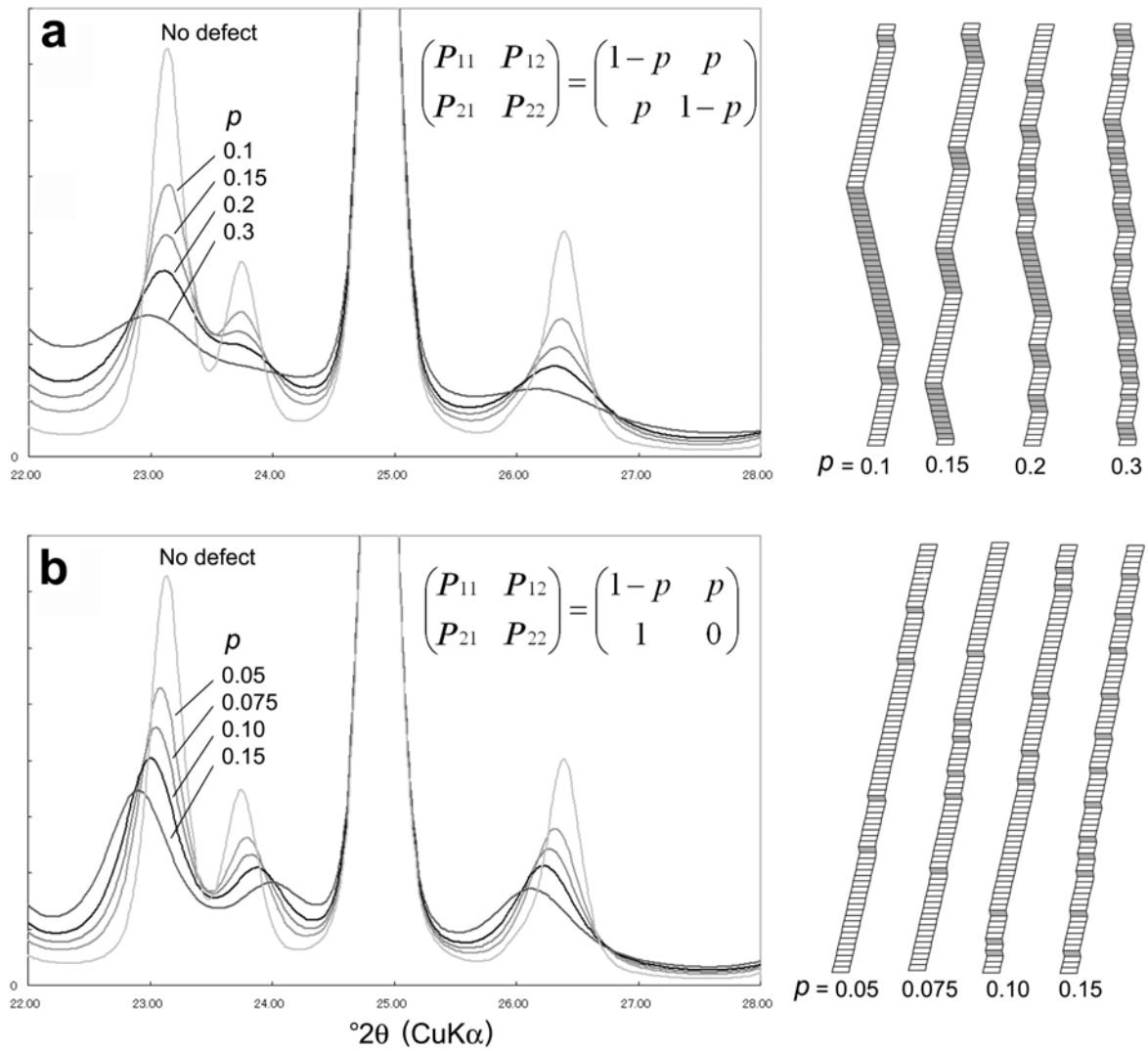


Figure 11. Simulations of the 02, 11 band in the XRD pattern with various degrees of stacking disorder expressed by p in the junction probability (P_{ij}) matrix shown in the figure. The columns to the right are schematic illustrations of examples of the stacking, drawn with the p parameter and randomizer function: (a) enantiomeric twin model; (b) isolated faults model (see the text for detail).

ET-disordered ones (Figure 11a). However, the profiles of these reflections are considerably asymmetric (Figure 1b) which may be explained by the addition of shifted peaks by the disorder with IF mode to non-shifted peaks. Such asymmetries of 021, $0\bar{2}1$ peaks were also found in XRD patterns of kaolinite with a similar Hinckley index in previous works (Plançon *et al*., 1988, 1989). Together with the results of SAED (Figure 3) and HRTEM, the profiles of the 02, 11 band reflected primarily a mixture of grains with various degrees and modes of disorder with alternating $\boldsymbol{t}_1$ and $\boldsymbol{t}_2$ layer displacement, which is considered the most abundant defect type.

The formation of the disordered structure with ET mode seems natural. During layer-by-layer growth of kaolinite, stacking of a new layer with the same layer displacement as that of the preceding layer is probably favored energetically compared to that with a different layer displacement. This led to small P_{12} values (<0.5) in the calculation of the ET mode. On the other hand, the origin of the fault structure with IF mode was not straightforward. As stated by Bookin *et al*. (1989), the faults can be introduced by an external shear force applied after kaolinite crystals formed. Capim kaolinite may have experienced a geologic shear force. Such asymmetric peaks were also generated experimentally by long and intense grinding of kaolinite (Reynolds and Bish, 2002). The asymmetric character in the present specimen was not induced in this way because grinding was minimal (Johnston *et al*., 2008). Another possibility is that the crystals were formed by spiral growth mechanism to memorize the stacking sequence through

https://doi.org/10.1346/CCMN.2010.0580106 Published online by Cambridge University Press

the crystal. In this case, stacking faults can be inserted by the formation of extrinsic two-dimensional nuclei with different layer displacement on the spiral surfaces, or by the occasional invasion of the ridge from neighboring spirals with different layer displacement (Kogure and Nespolo, 1999).

Stacking faults with the displacement of octahedral vacancy sites and/or $n60^{\circ}$ layer rotation were also found in the specimen, although they were less common than those related to alternating $\boldsymbol{t}_1$ and $\boldsymbol{t}_2$ layer displacements. Johnston *et al*. (2008) reported that low-temperature FTIR spectra from a number of kaolinite specimens, including the present one, showed absorption bands that can be ascribed to dickite and nacrite. One of the objectives of the present study was thus to establish whether these polytypes exist as separate crystals or as local stacking sequences in the kaolinite matrix. Among a number of SAED patterns taken during the experiment, none showed two-layer periodicity as evidence of dickite or nacrite. Hence, together with the results from Figures 7–10, the absorption bands in the FTIR spectrum may correspond to stacking faults inducing structural fragments similar to dickite or nacrite in the main kaolinite structure. On the other hand, the XRD pattern (Figure 1a) shows peaks that can be assigned to dickite (023 and $\bar{1}14$), indicating that the dickite phase may exist as separate crystals in the specimen. However, the peaks for dickite are weak, and intense characteristic peaks for dickite are absent from the experimental pattern. For instance, 022 at 23.5º2θ should be observed at the midpoint between the two kaolinite peaks for $0\bar{2}1$ (23.1º) and 021 (23.8º), or the inter-peak intensity between the two kaolinite peaks should be greater than others in the 02, 11 band in the patterns. Hence, the two observed peaks are probably related to other impurities. With respect to nacrite, major peaks for $\bar{3}14$, 022, and 310 should appear between 36.5 and 38º2θ but the experimental pattern is almost flat in this region. However, the volume of nacrite seemed so small, from the FTIR spectrum, that characteristic peaks of nacrite may not be detected in the XRD pattern.

CONCLUSIONS

The majority of stacking disorder in sedimentary kaolinite from Capim, Brazil, is related to the alternation of $\boldsymbol{t}_1$ and $\boldsymbol{t}_2$ layer displacements. However, faults induced by the displacement of octahedral vacancies and/or by $n60^{\circ}$ layer rotations, thus locally forming dickite/nacrite-like fragments, were occasionally observed in HRTEM images. Electron diffraction suggested the existence of faults corresponding to (0 or $\pm\boldsymbol{b}/3$) layer displacements and/or to $(2n+1)60^{\circ}$ layer rotation between adjacent layers, suggesting the existence of nacrite-like stacking. These local dickite/nacrite-like fragments may be responsible for the ν(OH) absorption bands ascribed to dickite and nacrite in a low-temperature FTIR spectrum reported by Johnston *et al.* (2008). With respect to the disorder induced by alternating $\boldsymbol{t}_1$ and $\boldsymbol{t}_2$ layer displacements, two extreme modes (isolated faults and enantiomeric twins) were observed in the HRTEM images. The former is probably related to the asymmetric peak profile of several reflections in the 02, 11 band of the XRD pattern.

ACKNOWLEDGMENTS

The authors are grateful to V.A. Drits and M. Mellini for their valuable suggestions and comments on the manuscript, and to B. Lanson (AE) for editorial handling of the manuscript.

REFERENCES

Bailey, S.W. (1963) Polytypism of the kaolin minerals. *American Mineralogist*, **48**, 1196–1209.

Bish, D.L. and Von Dreele, R.B. (1989) Rietveld refinement of non-hydrogen atomic positions in kaolinite. *Clays and Clay Minerals*, **37**, 289–296.

Bookin, A.S., Drits, V.A., Plançon, A., and Tchoubar, C. (1989) Stacking faults in kaolin-group minerals in the light of real structural features. *Clays and Clay Minerals*, **37**, 297–307.

Brindley G.W. and Robinson, K. (1946) Randomness in the structures of kaolinitic clay minerals. *Transactions of the Faraday Society*, **42B**, 198–205.

Ehrenberg, S.N., Aagaard, P., Wilson, M.J., Fraser, A.R., and Duthie, D.M.L. (1993) Depth-dependent transformation of kaolinite to dickite in sandstones of the Norwegian Continental Shelf. *Clay Minerals*, **28**, 325–352.

Giese, R.F. (1988) Kaolin minerals: structures and stabilities. Pp. 29–66 in: *Hydrous Phyllosilicates (Exclusive of Micas)* (S.W. Bailey, editor). Reviews in Mineralogy, **19**, Mineralogical Society of America, Washington D.C.

Hinckley, D.N. (1963) Variability in crystallinity values among the kaolin deposits of the coastal plain of Georgia and South Carolina. *Clays and Clay Minerals*, **11**, 229–235.

Johnston, C.T., Kogel, J.E., Bish, D.L., Kogure, T., and Murray, H.H. (2008) Low-temperature FTIR study of kaolin-group minerals. *Clay and Clay Minerals*, **56**, 470–485.

Kilaas, R. (1998) Optimal and near-optimal filters in high-resolution electron microscopy. *Journal of Microscopy*, **190**, 45–51.

Kogure, T. and Inoue, A. (2005a) Determination of defect structures in kaolin minerals by high-resolution transmission electron microscopy (HRTEM). *American Mineralogist*, **90**, 85–89.

Kogure, T. and Inoue, A. (2005b) Stacking defects and long-period polytypes in kaolin minerals from a hydrothermal deposit. *European Journal of Mineralogy*, **17**, 465–473.

Kogure, T. and Nespolo, M. (1999) A TEM study of long-period mica polytypes: determination of the stacking sequence of oxybiotite by means of atomic-resolution images and Periodic Intensity Distribution (PID). *Acta Crystallographica*, **B55**, 507–516.

Kogure, T., Hybler, J., and Ďurovič, S. (2001) A HRTEM study of cronstedtite: determination of polytypes and layer polarity in trioctahedral 1:1 phyllosilicates. *Clays and Clay Minerals*, **49**, 310–317.

Kogure, T., Eilers, P.H.C., and Ishizuka, K. (2008) Application of optimum HRTEM noise filters in mineralogy and related sciences. *Microscopy and Analysis*, **22**, S11–S14.

Marks, L.D. (1996) Wiener-filter enhancement of noisy HREM images. *Ultramicroscopy*, **62**, 43–52.

https://doi.org/10.1346/CCMN.2010.0580106 Published online by Cambridge University Press

Murray, H.H. (1954) Structural variations of some kaolinites in relation to dehydrated halloysite. *American Mineralogist*, **39**, 97–108.

Plançon, A. (2001) Order-disorder in clay mineral structures. *Clay Minerals*, **36**, 1–14.

Plançon, A. and Tchoubar, C. (1977) Determination of structural defects in phyllosilicates by X-ray powder diffraction – II. Nature and proportion of defects in natural kaolinites. *Clays and Clay Minerals*, **25**, 436–450.

Plançon, A. and Zacharie, C. (1990) An expert system for the structural characterization of kaolinites. *Clay Minerals*, **25**, 249–260.

Plançon, A., Giese, R.F., and Snyder, S. (1988) The Hinckley index for kaolinites. *Clay Minerals*, **23**, 249–260.

Plançon, A., Giese, R.F., Snyder, R., Drits, V.A., and Bookin, A.S. (1989) Stacking faults in the kaolin-group minerals – defect structures of kaolinite. *Clays and Clay Minerals*, **37**, 203–210.

Reynolds, R.C. and Bish, D.L. (2002) The effects of grinding on the structure of a low-defect kaolinite. *American Mineralogist*, **87**, 1626–1630.

Sousa, D.J.L., Varajão, A.F.D.C., Yvon, J., and Da Costa, G.M. (2007) Mineralogical, micromorphological and geological evolution of the kaolin facies deposit from the Capim region (northern Brazil). *Clay Minerals*, **42**, 69–87.

Treacy, M.M.J., Newsam, J.M., and Deem, M.W. (1991) A general recursion method for calculating diffracted intensities from crystals containing planar faults. *Proceedings of the Royal Society of London A*, **433**, 499–520.

Zvyagin, B.B. and Drits, V.A. (1996) Interrelated features of structure and stacking of kaolin mineral layers. *Clays and Clay Minerals*, **44**, 297–303.

(*Received 26 March 2009; revised 31 August 2009; Ms. 298; A.E. B. Lanson*)

https://doi.org/10.1346/CCMN.2010.0580106 Published online by Cambridge University Press